Metascience in Aerospace

Metascience in Aerospace, 2(2): 15–41.
DOI: 10.3934/mina.2025002
Received date: 29 November 2024
Revised date: 08 May 2025
Accepted date: 26 May 2025
Published date: 13 June 2025

https://www.aimspress.com/journal/mina

Research article

Electric generating thrust vectors of arial vehicles via onboard centrifugal force modulation - Fact or Fake?

Wolfgang Holzapfel*

Faculty of Mechanical Engineering, University of Kassel, 34109 Kassel, Germany

* **Correspondence:** Email: wolfgang.holzapfel@uni-kassel.de.

Abstract: This paper deals with a novel method for electrically propelling aerial vehicles (AVs). The technique utilizes the rotational energy stored in gyro rotors that are electrically charged before the start-up process, converting it into forward thrust for the AV. This conversion is achieved by generating specific centrifugal force pulses through brief rotor unbalances Precise control over the timing and spatial extent of these unbalances is crucial for efficient thrust generation. Our initial concept of controlled unbalance propulsion (CUP) suggests that it is feasible to obtain thrust vectors for various types of rotor-driven AVs. Particularly for small unmanned aerial vehicles (UAVs), significant translational accelerations and speeds can be achieved, potentially reaching orbital velocities. This approach may also enable energy-efficient levitation of UAVs. The paper proposes certain aerodynamic considerations for rotor-driven aerial vehicles. We present tangible evidence in this paper that supports the grounded physics principles of pulsed centrifugal propulsion, demonstrating its viability with current advanced technologies.

Keywords: electrical vehicle propulsion; high-speed rotors, energy storage/conversion; controlled unbalance; centrifugal force modulation; unmanned aerial vehicles

1. Introduction

Electrical thrust generation via centrifugal force modulation represents, to our knowledge, the first attempt at quantitative designing a centrifugal force drive that (1) utilizes flywheel energy storage and (2) transfers that energy by controlled flywheel unbalance modulation into vehicle movement [1]. Thus, the flywheel on board the vehicle also serves for energy storage as well as for vehicle propulsion. It has been shown that a basic requirement for a functional thrust generation is predicated on the precise spatial rectification of the vector of the resulting centrifugal force. This, in turn, can be achieved by a rapid temporal impulse modulation of unbalance-induced force amplitudes as described in detail in the paper.

The concept of propulsion generated through rotating unbalance is not a novel idea. The patent literature already contains several proposals for what are known as centrifugal force drives that suggest using rotors with an uneven mass distribution, e.g., [2–4]. However, no practical implementations of these ideas have been achieved thus far. The scientific community finds these methods contentious, primarily because they appear to contravene the law of conservation of momentum and because the rotating centrifugal force, being a pseudo-force, is unlikely to provide a sustained translation of the rotor's center of mass. To date, there seems to be an absence of contributions or dialogues concerning this topic in recognized scientific journals. Moreover, current reviews of various propulsion technologies for unmanned aerial vehicles (UAV) in publications [5–7] do not mention this inertial technology. Conversely, it is widely acknowledged that the rotational energy of masses can be effectively used for energy storage, as demonstrated, for instance, in [8–13]. For a current perspective on the design and optimization of flywheel energy storage systems within modern automotive engineering, see [14].

To properly understand the functionality of these drives and address the fundamental challenges associated with flywheel propulsion, it is essential to consider the pertinent physical principles and laws [15–17]. The law of conservation of angular momentum dictates that within a closed rotational system, the total angular momentum remains constant, provided that no external forces are acting on it. This means that in the absence of external forces, the angular momentum does not change. However, if an external force leads to an acceleration of the system's mass, this causes a change in the angular velocity and consequently affects the angular momentum.

On the other hand, there is no overarching conservation law for rotational energy because rotational energy is influenced by the specific forces and torques applied to the system. In the absence of external forces or torques, the rotational energy stays constant. However, when forces or torques are applied and bring about linear acceleration, rotational energy can be transformed into translational energy. If rotational energy is transformed into other kinds without altering the system's angular momentum, either the moment of inertia or the axis of rotation must change. Conversely, if both the rotational axis and the moment of inertia remain unchanged, then changing the form of rotational energy will lead to a modification of the system's angular momentum. This happens because changes in rotational energy are linked to variations in angular velocity.

In classical physics, only forces that act on an object from external sources are considered to be "real" forces. These external forces result from direct interactions between objects and can be described by laws such as gravity or Coulomb's law. However, in accelerating reference frames—whether translationally or rotationally—additional forces arise, such as inertial force, centrifugal force,

Coriolis force, and Euler force. Reference systems that are free from acceleration, known as inertial reference systems, do not experience these additional forces.

During the 19th century, physics considered these forces to be "pseudo-forces" because they arose from mathematical transformations in noninertial frames, rather than from direct physical interactions. Specifically, centrifugal forces are considered internal reactions occurring in rotating systems. They do not alter the total momentum of the system because they are internal forces.

According to the conservation of momentum, if no external forces act on a system and its energy remains constant, the total momentum of the system also remains unchanged. This principle suggests that internal forces like inertial propulsion forces cannot alter the system's momentum to achieve net propulsion. Consequently, reliance on such forces for propulsion, without external interactions or energy considerations, would not yield a technically useful propulsion system.

The discussion referenced highlights a shift in understanding how forces traditionally considered to be "pseudo-forces", such as centrifugal forces, can have tangible, impactful effects in real-world systems, like causing material failures of rotors in engineering and influencing atomic interactions. While classical physics often viewed these forces as results of noninertial reference frames and not directly part of the fundamental interactions, their real-world impact necessitates treating them as significant influences, particularly in engineering contexts.

In this framework, the aim is to harness centrifugal forces for propulsion by controlling their direction and magnitude. This involves converting the rotational energy of a system into directed translational energy through techniques like rectification and pulse amplitude modulation, timed precisely with the system's rotation. By doing so, it is hypothesized that centrifugal forces could be used to propel and maneuver AVs.

This methodology proposes that targeted manipulation of a system's rotational dynamics and symmetry can free linear momentum from conservation enforcement, effectively using these forces for propulsion. However, this idea remains a hypothesis that needs rigorous testing and validation. The outlined paper structure reflects a methodical approach to explore this concept, starting with the foundational theory (Section 2), then deriving energy conversion formulas and system configurations (Section 3) to get rough estimates of the flight performance potential of the novel propulsion systems (Section 4). Next, in Section 5, we evaluate the ability of rotor-driven AVs in terms of maneuverability and levitation. A necessary discussion of engineering applications and requirements like material strength and precise unbalance control is provided in Sections 6 and 7. In Section 8, some special aerodynamics aspects of rotor-driven aerial vehicles are discussed. Finally, our conclusions on the feasibility of pulsed propulsion of AVs are presented in Section 9.

Such an approach attempts to bridge theoretical considerations and practical engineering implementations, recognizing the complex interplay of forces in noninertial frames while seeking to harness those effects for tangible technological advancements.

2. Foundational theory of propulsion generation by means of controlled rotor unbalances (CUP)

Let us consider a stiff rotor disc with a radius R, a thickness D (where $D < R$), and a homogeneous material distribution, having a total mass M. This disc is equipped with a fixed unbalanced mass m_u located at its periphery, as depicted in Figure 1. The disc's rotational axis A is perpendicularly centered

within a planar coordinate system defined by orthogonal axes (x, y), which are fixed in an inertial reference frame. In the discussion that follows, we will utilize the equivalent circuit mass point diagram shown in Figure 1 (right) for analysis**.**

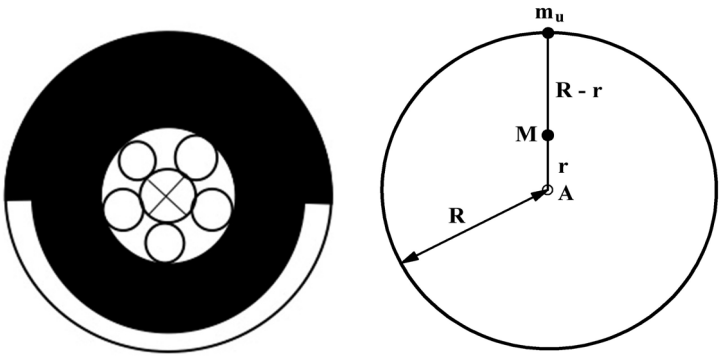

Figure 1. left: Unbalanced rotor due to asymmetric mass distribution. Right: Equivalent circuit mass point diagram [17]. A, rotation axis, perpendicular to the paper plane (x;y); m_u, point of the unbalanced mass; M, point of the rotor disc's mass; R, rotor radius; r, translation of M due to m_u.

Due to disc rotation, the generated centrifugal force vector, written in polar coordinates, is

$$\underline{F_u} = \underline{R}\, m_u\, \omega^{2} \qquad (1)$$
$$\underline{R} = R\, exp\{i\,(\omega\, t + \varphi_0)\}$$

with the following magnitudes:

$\underline{R}$ radius vector (i = imaginary unit) pointing from axis A to unbalanced mass m_u;
φ_0 rotor fixed azimuth of the unbalanced mass point m_u;
R radius of rotor disc;
$\omega = 2\pi f$ (angular) revolution frequency;
$T = 1/f$ cycle time of rotor disc.

Equation 1 says that the centrifugal force vector $\vec{F}_u$ is always pointing in direction of the instantaneous $\vec{R}$. Its magnitude F_u increases proportionally with m_u and proportionally with the rotor radius R; furthermore, F_u is increasing quadratically with the applied rotor rotation frequency f.

It is useful to introduce unbalance vector $\vec{U}$, which is the vector $\vec{F}_u$ divided by the square of angular rotation frequency ω

$$\underline{U} = U_0\, e^{\,i(\omega\, t + \varphi_0)} = m_u\, R\, e^{\,i(\omega\, t + \varphi_0)} \qquad (2)$$

Note, the magnitude of unbalance $U_0 = m_u R$ is independent of ω.

Due to the peripheric unbalanced mass m_u, there is a small displacement r when the disc's center of gravity M rises, away from rotor rotation axis A. Note, this displacement is caused due to the static balancing of the rigged disc. Additionally, the elasticity and strain of real rotor materials may contribute to real displacement, but we will not take this effect into account here.

In the case of a very small unbalanced mass m_u (i.e., $M = M_0 + m_u$, $m_u << M_0 \cong M$), the following vector equation results:

$$M \underline{r} = m_u \underline{R} \tag{3}$$

respectively, for the magnitudes

$$M r = m_u R$$

According to Eq 3, the displacement r always points towards the peripheric unbalanced mass m_u. Thus, the rotation axis A, disc mass M, and unbalanced mass point m_u are located on the same radius vector $\underline{R}$ (azimuth φ_0). Considering this, we draw the following conclusion: The vectorial displacement r of the center of gravity M can be controlled in principle by choosing the magnitude and azimuth of the peripheric unbalanced mass m_u.

Now the question arises: Is this mass displacement effect insignificantly small or can it be used to the best advantage in propulsion technology?

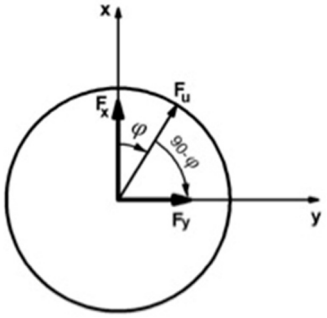

Figure 2. Components of the centrifugal force vector. (F_u: instantaneous centrifugal vector; F_x: effective x-component of F_u. F_y: noneffective-component of F_u.: φ instantaneous rotation angle of F_u against x).

To give the answer, in Figure 2, the centrifugal force F_u is represented as in two orthogonal components:

$F_{ux} = F_u \cos \varphi_x$ (effective centrifugal force component; see below) (4)

$F_{uy} = F_u \sin \varphi_x$ (noneffective centrifugal force component; see below). (5)

$\varphi_x = \omega t \pm mod\ 2\pi$ instantaneous phase angle

t = 0: $\varphi_x = 0$

$t = T$: $\varphi_x = 2\pi$

Both components describe strictly harmonic forces having zero averages over each rotation period, i.e.

$$F_x = (1/2\pi) \int_0^{2\pi} Fux d\varphi = 0$$

$$F_y = (1/2\pi) \int_0^{2\pi} Fux d\varphi = 0$$

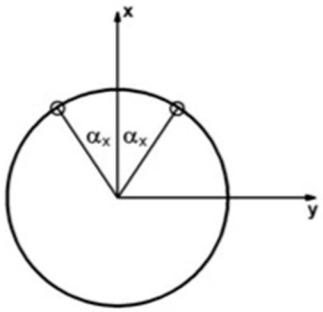

Figure 3. Active angle interval $2\alpha_x$. (symmetric to the thrust direction x).

Our approach to achieving nonzero translational propulsion of a rotating disc involves the (partial) rectification of the centrifugal forces. To illustrate the necessity of force rectification, let us consider the desired propulsion direction to be along the x-axis. Therefore, during each rotation, the unbalance must be modulated as box function, namely (refer to Figure 3):

1. In an azimuthal angle region of α_x, which is highly symmetric about the x-axis (the desired propulsion direction), we generate a nonzero unbalance.

2. Outside of this region, i.e., in the remaining angle $2\pi - 2\alpha_x$, the unbalance is consistently compensated.

Within the time period τ, which is a small fraction of the total cycle time T,

$$\tau / T = 2\alpha_x / 2\pi \tag{6}$$

we must rapidly switch the rotor's unbalance on and off. This is accomplished by employing rotor-fixed actuators that can generate specific unbalances. The resultant pulsating centrifugal forces provide directed propulsion of both the rotor mass and the overall flying object through the rotor bearings.

If we manage this ultrafast modulation in sync with the rotation, it generates a series of force impulses. Each impulse has a duration τ and is separated by the cycle time T. This train of impulses causes a significant change in the translational motion of the rotor mass M. According to Newton's second law, the force F acting on a mass point M is equal to the derivative of its translational momentum $P = Mv$, where v is the translational velocity:

$$\begin{aligned} dP/dt &= F(t) \\ \Delta P &= M\Delta v = F(t)\,\Delta t \end{aligned} \tag{7a}$$

The resulting impulse change during each rotation follows from

$$\Delta P = \int_{-\tau/2}^{\tau/2} F(t)dt \tag{7b}$$

1st) For the (ineffective) y-component $F_{uy} = F_u sin\ \varphi_x$ of centrifugal force, zero average of impulse change is confirmed:

$$\Delta P_y = \int_{-\tau/2}^{\tau/2} Fuy\ dt\ =\ 0$$

2nd) We get for the effective impulse component (x-component) of centrifugal force:
$F_{ux} = F_u \cos \varphi_x$.

$\Delta P_x = \Delta P = \int_0^T Fu \cos\omega t \, dt = 2\int_0^{\tau/2} Fu \cos\omega t \, dt$

According to formula (6) we introduce the non-zero force magnitude F_x :

$$\Delta P_x = \tau F_x = 2(Fu / \omega) \sin(\omega\tau/2) \quad (8)$$

Let us substitute in (8) via box function Eq. (6) to get the dependence on the angle α of unbalance activity:

$$F_x = F_u (\sin(\alpha_x) / \alpha_x) = F_u \, sinc(\alpha_x) = R\omega^2 m_u \, sinc(\alpha_x) \quad (9)$$

Here, the function sinc (α_x) is the Fourier transform of the unbalance box function described by (6). Some values of sinc (α_x) within the α_x-range of our interest ($0 \leq \alpha_x \leq \pi / 2$) are: $sinc(0) = 1$; sinc $(\pi/4) = 2(2^{1/2}) / \pi$; $sinc(\pi/2) = 2/\pi$; $sinc(\pi) = 0$

Based on the equations provided in the text above, we can summarize the following points:

1. Directed propulsion force F_x is straight proportional to unbalance force F_u. The proportional factor is given by function $sinc(\alpha_x) = \sin(\alpha_x) / \alpha_x$. Because, the activity angle $\alpha_x = \pi \tau / T$ depends on the quotient of activation time τ of the unbalance generator and rotation time T of the rotor, the sinc - function increases to value 1with decreasing rotation frequency f.

2. Within the α_x-range of our interest the proportional factor sinc is between 1 and 2/3. We are allowed to conclude, the magnitudes of F_x and F_u have the same dimension. Thus, for small activity angles α_x the propulsion force F_x can be simply approximated by the product of rotor radius (R), unbalance mass (m_u), and square of rotational frequency (f). This approximation will be used later in chapter 4.

3. By intermittently activating the rotor unbalance, only the desired outward force component (F_x) - the propulsion force - occurs in the rotation plane. This force is orthogonal to the rotation axis (A) and precisely points in the desired direction (x), which is symmetrically positioned within the unbalance activity angle $2\alpha_x$.

4. The orthogonal force component (F_y) is eliminated during each rotation period, focusing the propulsion force solely in the desired direction.

5. In the absence of other restrictions, the unchained rotor will move precisely in the direction x of the acting propulsion force (F_x), starting from $x = 0$ at time $t = 0$.

These points highlight the key factors influencing the propulsion force generated by the rotor system and the directional control achieved through controlled unbalance activation.

Here is a description of the takeoff scenario:

The AV, equipped with a well-balanced rotor, is initially secured in a constraining device at the starting position. Once electrically charged, the rotor begins to spin at a high rotational frequency. At the onset of the takeoff phase, the translational energy of the fixed rotor is zero because all the kinetic energy is stored as rotational energy. Introducing a constant unbalanced mass on the spinning rotor would result only in a rotating centrifugal force, leading to unwanted vibrations in the UAV's structure and the constraining device. However, by activating and deactivating the unbalance at specific angular intervals during each revolution, a sequence of force pulses in the desired direction can be generated.

This technique leverages continuous rotation to produce controlled, directed propulsion. Once the constraining device is released, this sequence of directed force pulses generates translational acceleration, enabling the AV to move away from its initial position.

In simplifying the dynamic scenario, we assume that the rotor system operates below its critical speed, where the lowest resonance frequencies are higher than the rotor's rotational frequency f. Critical components like unbalance actuators and rotor bearings are considered to be rigid, eliminating additional elastic and friction forces in the system model. In flight, only inertial forces affect the rotor bearings, since elastic mounting forces are absent once the rotor is detached. This results in significantly reduced bearing loads from unbalance during flight compared with tethered rotor operations, thereby prolonging bearing lifespan.

3. Conversion of rotational energy into translational vehicle energy

Pulsed propulsion by centrifugal force modulation can be applied in two modes of energy management (see Figure 4).

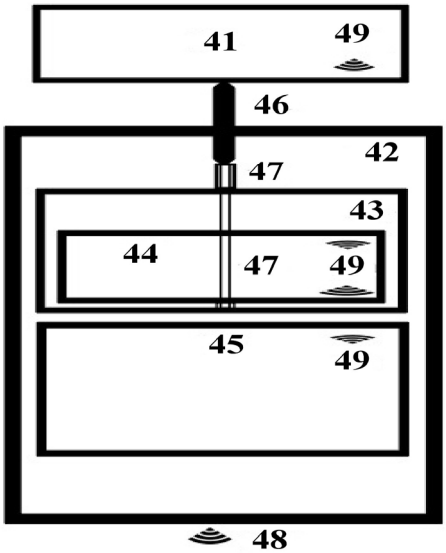

Figure 4. Minimal configuration of the rotor propulsion system. 41, Drive generator, switchable in the startup phase or permanently on board; 42, vehicle cell; 43, vacuum capsule for housing the high-speed rotor (44) with controlled unbalance; 45, unbalance vector control; 46, power transmission generator/rotor; 47, rotor's rotation axis; 48, radio connection to the terrestrial control computer; 49, onboard telemetries.

(1) The rotor could be used with an integrated onboard drive and is able to deliver high and sustained electrical power output during the complete mission. A low weight and compact design for such a combined power/propulsion system that is well suited for use onboard a small AV must be achieved here, which is not an easy engineering task. Generally, controlled unbalance propulsion (CUP) involving a combination of inertial and electric energy stored onboard vehicles is viable. In this system,

the unbalance-controlled rotor is integrated into an electric motor drive/generator circuit. Initially, extra electrical power is stored in lightweight onboard batteries during the prestart phase, concurrently with loading the rotor electrically to its maximum rotational frequency, ω_0. Subsequently, during flight, the stored electrical energy can compensate for the decrease in rotational energy during the thrust phases, enabling the rotor to maintain a constant frequency, for instance ω_0, during the vehicle's operation. This could lead to streamlined guidance software and energy management. Moreover, with the augmented onboard energy capacity, there is the chance to extend the operational range of the vehicle.

(2) Alternatively, the rotor will be brought to operating speed before takeoff through temporary mechanical coupling with a powerful external electric motor. The advantage of this pure inertial energy storage is the much lower weight and greater simplicity of the onboard propulsion system. It seems to be better suited for small UAVs. The critical question must be answered about whether there is enough energy onboard such inertial AVs and how much flight performance and maneuverability are limited. In the following, we focus on this second energy mode because it seems to be better suited for a fundamental understanding of the interplay of onboard energy management and flight performance. Details of the modes will be discussed in a future paper.

When discussing the conversion of rotational energy (E_{rot}) into translational energy (E_{trans}) in the context of an inertial UAV, it is important to consider the conservation of total kinetic energy (E_0) onboard the vehicle. According to the energy theorem, the total kinetic energy must remain constant. Therefore, we can express this conservation using the equation

$$E_0 = E_{rot} + E_{trans} = const. \tag{10}$$

At the beginning of the takeoff scenario, when the UAV is at the starting point (x = 0), the maximum rotational energy is available. This can be represented as

$$max\ E_{rot} = (1/2)\,\theta\,\omega o^2 = E_0 \tag{11}$$

with the moment of the disc inertia θ and the maximum rotation frequency ω_0:

$\theta = (1/2)\ M\ R^2$, *and* $\omega_0 = 2\ \pi f_0$.

According to (11), storable rotation energy increases proportionally with the rotor mass M and with the square of the disc radius R and the square of rotational frequency f_0. Thus, for a given size and material of the rotor disc, a doubling of its rotational frequency f_0 will result in quadrupling of the mechanically stored airborne energy. Our conclusion is that the store parameter f_0 is of high importance in flight performance evaluation. As per Equation (11), the amount of storable rotational energy increases proportionally with the rotor mass (M), the square of the disc radius (R^2), and the square of the rotational frequency f_0. Therefore, if the rotational frequency f_0 is doubled while keeping the size and material of the rotor disc constant, the mechanically stored airborne energy will quadruple. This highlights the significance of the rotational frequency (f_0) as a parameter in evaluating flight performance (refer to Section 4 for more details).

On the other hand, assuming ideal conditions in energy conversion (i.e., friction-free disc rotation and vehicle translation) and zero-gravity space, the potential maximum of translational energy appearing at end of energy conversion is given by

$$max\ E_{trans} = E_0 = \frac{1}{2} M'\ v_{max}^2 = M\ R^2\pi\text{^}2\ \ f_0^2 \tag{12}$$

This assumption is equivalent to 100 % efficiency in the conversion of the rotational energy to translational propulsion. It is also important to note that M' is larger than M, as M' represents the total mass of the UAV while M only represents the smaller mass of the rotor disc. The vehicle construction factor *C*, which is the ratio of *M´* to *M*, can be assumed to be between 1 and 2 in realistic scenarios.

Thus, the maximum translational velocity is as follows:

$$v_{max}^2 = (1/2)\, R^2\, \omega o^2\, M/M'$$

$$v_{max} = \frac{1}{\sqrt{2}}\, R\, \omega o\, (M/M')^{1/2} \tag{13}$$

The maximum velocity v_{max} depends on radius *R*, the angular velocity ω_0, and the construction factor $C = M'/M$; however, v_{max} is independent from the unbalanced mass m_u.

We look now at intermediate states of energy transformation. The energy theorem postulates that each increase in translational energy asks for an equal decrease in rotational energy, i.e.

$$-dE_{rot} = dE_{trans} \tag{14}$$

$$E_{rot} = (1/4)\, M\, R^2\, \omega^2 \tag{15}$$

$$dE_{rot} = (1/4)\, MR^2 2\, \omega\, d\omega = (1/2)\, MR^2 \omega d\omega \tag{16}$$

$$E_{trans} = (1/2)\, M'\, v^2 \tag{17}$$

$$(-1/2)\, MR^2\, \omega\, (d\omega/dt) = M'\, v\, (dv/dt) \tag{18}$$

$$(-1/2C)\, R^2\, \omega\, (d\omega/dt) = v\, a \tag{19}$$

Equation 19 teams our rotational magnitudes with the translational ones of interest, i.e., the vehicle's velocity v and its translational acceleration a.

Newton's Third Law (action = reaction) tells us about the acceleration *a* of mass. The centrifugal force $F = m_u R\, \omega^2$ caused by the unbalance and the inertial force $F = M'\, a = M'\, d^2x/dt^2$ acting on the vehicle mass's M´ must be in equilibrium, i.e.,

$$M'\, a = m_u R\, \omega^2 \tag{20}$$

Thus, we get the acceleration (**$a = dx^2/dt^2 = dv/dt$**) of the vehicle's mass *M'*:

$$a = (m_u/M')\, R\, \omega^2 \tag{21}$$

From (19), the time-dependent change in rotational frequency is as follows:

$$d\omega/dt = -2\, C\, v\, a/R^2\, \omega_0 = -2(m_u/M\, R)\, v\, \omega$$

$$d\omega/\omega = -2(m_u/M\, R)\, vdt \tag{22}$$

After integration, we have

$$ln\omega - ln\omega_0 = -2(m_u/M\, R) \int_0^{tx} vdt \tag{23}$$

$$ln\,(\omega/\omega_0) = ln\,(f/f_0) = -2(m_u/M\, R)\, x \tag{24}$$

We get the instantaneous rotational frequency dependent on x = x(t), which is the trajectory

length, depending on time of thrust t_x:

$$\omega = \omega_0 \exp\{(-2m_u/M\,R)\,x\},\ \text{resp.}\quad \omega^2 = \omega^2_0 \exp\{(-4mu/M\,R)\,x\}. \tag{25}$$

Rotational frequency decreases exponentially with increasing x(t). This follows from an increase in the translational energy and instantaneous velocity v (see Figure 5).

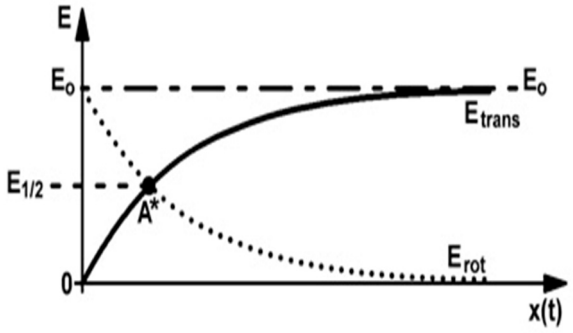

Figure 5. Decrease in rotational energy E_{rot} and increase in translational energy E_{trans} dependent on the flight path's length x(t). E_0, $E_{1/2}$ max and half-max of rotation energy, respectively; A*, point of energetic equivalence.

With (11) and (25), we get $E_0 = max\ E_{rot} = (1/4)\,M\,R^2\,\omega_0^2$

$$E_{trans} = (1/2)\,M'v^2 = (¼)MR^2\,\omega_0^2(1-\exp\{(-4mu/M\,R)\,x\}) \tag{26}$$

$$v^2 = (1/2C)\,R^2\,\omega_0^2(1-\exp\{(-4mu/M\,R)\,x\})). \tag{27}$$

$$v = (1/2C)^{½}\,R\,\omega_0\,(1-\exp\{(-4mu/M\,R)\,x\}))^{1/2} \tag{28}$$

where v(x) is the instantaneous velocity dependent on the trajectory length x. Setting x = 0 delivers the initial velocity v = 0 in accordance with our takeoff scenario above. From (28), we get, by differentiation, the instantaneous translational acceleration of the rotor

$$a = (m_u/M')\,R\,\omega^2 = (m_u/M')\,R\,\omega_0{}^2\exp\{(-4mu/M\,R)\,x\}) \tag{29}$$

The initial acceleration a_0 follows from (29) by setting the starting point condition x = 0

$$a_0 = (m_u/M')\,R\,\omega_0^2 \tag{30}$$

Both the instantaneous acceleration a and velocity v depend on the mass quotient m_u/M', which presents the main steering magnitude for propulsion control. Acceleration increases proportionally with m_u/M'.

Regarding the momentum and angular momentum laws during energy conversion, the rotational momentum constantly decreases due to the reduction in the rotational frequency, while the translational momentum increases in magnitude due to the energy conversion accompanying the increase in translational velocity. However, it would be inappropriate to speak of the conversion of momentum, as these quantities cannot be reconciled due to the different physical dimensions of angular and translational momentum. There is a certain analogy to the behavior of a nonconservative system

(e.g., a system with friction). Here, the law of conservation of energy applies, but not the law of conservation of momentum.

4. Evaluation of some basic UAV flight performance data

Our theory above applies to the five parameters *M, R, f, m_u,* and $C = M'/M$. The radius *R* and masses *M* and *M´* are assumed to be fixed parameters during flight which cannot be changed. The flight performance can be controlled by precisely adjusting the active unbalanced mass m_u (or m_u/M) and/or by adjusting the initial rotation rate f_0 at the start (or the actual rotation rate f during flight). In most cases, a high initial rotational frequency f_0 is desired to store a large amount of energy on board, making the key steering parameter m_u/M.

As derived in chapter 2, the thrust magnitude F_x approximately equals magnitude of centrifugal force F_u. Therefore, we are allowed here, to use the following simple formulas for evaluation of UAV flight performance data:

Mechanically stored energy

$$E_{rot} = MR^2\,\omega_0^2/4 \tag{31}$$

This formula calculates the amount of pure mechanical energy stored in the system. The energy storable on board depends on the square of the radius R and the square of rotational frequency f_0 and is proportional to the mass M of the rotor. Any electrical power supply on board is ignored here. There is no influence of the construction factor C on the magnitude of storable rotational energy.

Initial thrust

$$F'_0 = M'\,a'_0 \tag{32}$$

This formula calculates the initial thrust generated by product of the mass of the vehicle (M') and its initial acceleration (a'_0).

Initial acceleration

$$a'_0 = (m_u/M')\,R\,\omega_0^2 \tag{33}$$

This is determined by the magnitude of m_u and/or the rotational frequency f_0. Typical values of $m_u = M'10^{-4} – M'\cdot10^{-6}$ are assumed in the calculation here, while f_0 is variable and R is fixed by design.

Height of the vertex

$$h_{max} = R^2\,\omega_0^2\,g_E^{-1.} \tag{34}$$

A horizontal spin orientation of the rotor disc has to be assumed here. The height of the vertex is independent from the rotor's mass M and m_u.

Maximum velocity

$$v_{max} = R\,\omega_0/2^{1/2} \tag{35}$$

A vertical spin orientation of the rotor disc is assumed here. The maximum velocity is independent from the rotor's mass M and m_u.

In explaining the magnitudes h_{max} and v_{max} in the tables, we start with the formula for stored rotation energy $E_0 = MR^2\omega_0^2/4$ (see Eq. 11), and thus we derive the following:

- Height of the vertex h_{max}: All stored energy is transformed into potential energy in the gravitational field of the Earth, and thus $M' g_E h_{max} = E_0$.

- Maximum velocity v_{max}: All stored energy is transformed into translational energy, and thus we have zero thrust and $E_{trans} = (1/2)\, M' v^2_{max} = E_0$ (equipotential flight path).

For a preliminary evaluation of the system's potential in flight performance, here, we take three hypothetical UAVs of different sizes and masses, and calculate the height of the vertex, the initial thrust, the initial acceleration, and maximum velocity dependent on the initial rotation rate. Tables 1 to 4 (below) show the rounded flight performance data of different UAVs, calculated according to Eq. (31) – (35) by means of a hp 15C. The effect of air resistance is not taken into account here.

All data calculated here were obtained under the simplifying assumption $M = M'$, and thus $C = 1$. For evaluation of a specific vehicle, we have to specify $C > 1$. Thus, the initial acceleration a_0' and the initial thrust F'_0 of the complete vehicle will be reduced, because of the bigger vehicle mass M' compared with the rotor mass M. This is according to the equation $a\, M = a'\, M' = m_u\, R\, \omega^2$**.** For instance, assuming $C = 2$, the height of the vertex as well as the initial thrust of the vehicle are smaller, namely half the value of the corresponding rotor data. Additionally, navigating back to the Earth's surface and managing a safe landing needs energy, too. However, we see no serious limitation in the flight performance. Even the mini-rotor should reach considerable peak heights of several kilometers and more, depending on its starting rotational frequency f_0. The medium-sized rotor should reach flight altitudes of commercial aircraft at rotational speeds of 200 per second. With the heavy-sized rotor, heights and speeds should be achievable that promise orbital capabilities.

Table 1 to 4. Flight performance data of different UAVs, calculated according Eq. 31–35 by means of hp 15C. The effect of air resistance is not taken into account here.

Table 1. Mini-rotor.
(R = 0.125 m, M = 2 kg, mu = M ×.10^{-4}).

Frequency f_0	Hight of Vertex h_{max}	Thrust F_0	Acceleration a'_0	Velocity v_{max}
100/s	0.160 km	10 N	5 m/s^2	55 m/s
200/s	0.640 km	40 N	20 m/s²	110 m/s
400/s	2. 550 km	160 N	80 m/s²	220 m/s
800/s	10 200 km.	640 N	320 m/s².	440 m/s
1000/s	15.940 km	1000 N	500 m/s^2	555 m/s

Table 2. Medium-sized rotor.
(R = 0.5m, M = 10 kg (material density ρ= 10 g/cm^3), m_u = M ×·10^{-4})

Frequency f_0	Hight of Vertex h_{max}	Thrust F_0	Acceleration a'_0	Velocity v_{max}
100/s	2,5 km	200 N	20 m/s²	220 m/s
200/s	10 km	800 N	80 m/s²	440 m/s
400/s	40 km	3200 N	320 m/s².	880 m/s
800/s	160 km	12 800 N	1280 m/s².	1760 m/s
1000/s	250 km	20 000 N	2000 m/s2	2220 m/s

Table 3. Heavy rotor.
(R = 2 m, M = 160 kg, mu = 16 g)

Frequency f_0	Hight of Vertex h_{max}	Thrust F_0	Acceleration a'_0	Velocity v_{max}
100/s	40 km	12 800 N	80 m/s²	850 m/s
200/s	160 km	5 1200 N	320 m/s².	1700 m/s
400/s	640 km	20 5000 N	1280 m/s².	3400 m/s
800/s	2560 km	82 0000 N	5120 m/s².	6800 m/s
1000/s	4000 km	128 0000 N	8000 m/s2	8500 m/s

Table 4. Heavy rotor.
(Same parameter set as above, but suited for human-sized flight mode: mu /M = 10^{-6})

Frequency f_0	Hight of Vertex h_{max}	Thrust F_0	Acceleration a'_0	Velocity v_{max}
100/s	10 km	12 8 N	0.8 m/s²	850 m/s
200/s	40 km	5 12 N	3.2 m/s².	1700 m/s
400/s	160 km	2.050 N	13 m/s².	3400 m/s
800/s	640 km	8.200 N	51 m/s².	6800 m/s
1000/s	1000 km	12.800 N	80 m/s2	8500 m/s

The increase in acceleration and inertial thrust is proportional to the increase in ω^2. In most cases the UAV user will not need really such high accelerations Thus, the steering parameter mu/M can be reduced during the start phase (for instance, to 10^{-6}; see above for the heavy-sized rotor in human-sized flight mode) and thus the rotational energy on board can be saved for later maneuvers.

Let us compare some of the calculated data with traditional propulsion methods:

The maximum thrust of the heavy rotor (R = 2 m, $m_u/M = 10^{-4}$, 1000 Hz) in the launch phase would be approximately that of all four engines of a Boeing 747-100 or that of the first stage (Vulcain) of an Ariane 5 rocket without boosters. If the same rotor operates in human-sized flight mode ($m_u/M = 10^{-6}$), the maximum thrust is reduced by a factor of 100, yielding a thrust of 12,800 N. These thrusts will be reduced to 1/e after a flight path length of 10 km (respectively, 1000 km), which is due to the decrease in rotational frequency as predicted in Formula (25).

The performance increase of the bigger rotors is easily explained. The maximum height h_{max} of the rotor depends on the product of the squared radius R and the squared rotational frequency f_0, but h_{max} is independent of the rotor mass M and steering parameter mu/M. Therefore, our theory says, for instance, that the vertex height of the heavy rotor will be about 256 times larger than the vertex height of the mini-rotor, assuming same parameter values (m_u/M and f_0) for both rotors. Note that the translational velocity depends also on the product $R\,f_0$, but linearly. Here, the maximum velocity increases from 570 m/s (mini-rotor) to 2.2 km/s (medium rotor) to 8.5 km/s (heavy rotor); all values were calculated for the top frequency 10^3/s.

We conclude here that controlled unbalance propulsion (CUP) of UAVs could provide excellent flight performance data. Our calculations let us hope that high thrusts and vehicle velocities up to orbital levels could be achieved. Thus, the working range of CUP drones could be extended to near-Earth space and is not limited to the Earth's atmosphere.

5. Maneuverability of the rotor and levitation in a gravitational field

In this section, we discuss some gyro-dynamic aspects of rotor-driven aerial vehicles and how pointing of the thrust vector could be changed. Here, a clear distinction must made between two states: Horizontal flight and vertical flight. The orientation of the rotor's axis of rotation at takeoff determines the flight state. Due to the principle of propulsion, the axis of rotation must always be perpendicular to the future plane of movement in which the translational displacement of the rotor will occur. Within this plane of movement, the flight direction is determined by the position of the rotor sector in which the unbalance is activated, specifically by the bisector of this rotor sector. This position can be adjusted through the electrical control of the unbalance and can therefore be easily changed. The new position of the bisector can be set within a single rotation of the rotor, if necessary, potentially in milliseconds. This allows for rapid changes in direction of the UAV within the x, y plane of movement (e.g., horizontal curved flight with a constant vertical axis direction). By reversing the thrust, the aircraft can also decelerate (potentially with a subsequent change in flight direction) by electrically rotating the active rotor sector by 180 degrees relative to the previous direction of propulsion. In principle, no aerodynamic actuators are required to initiate these yaw and braking maneuvers.

During changes in attitude of a rotor-driven aircraft, gyroscopic forces can occur, which couple with the movements around the aircraft's axes, and their influence on the flight motion must be taken into account. Here is an example. After takeoff and before landing, it is necessary to tilt the rotor's axis of rotation by 90^0 to transition from horizontal flight to vertical flight (or vice versa). This requires a rotation around the pitch axis, which is oriented perpendicular to the direction of propulsion and the vertical axis of rotation. In this transition phase, gyroscopic forces occur because the law of conservation of angular momentum opposes the change in direction. This also applies to rolling. Only in yawing (as described above), the angular momentum remains directionally stable, and disruptive gyroscopic forces cannot occur.

There are generally two methods for maneuvering under the influence of gyroscopic forces:

1. Utilization of gyroscopic forces;
2. Compensation for gyroscopic forces.

For Method 1, the utilization of gyroscopic forces refers to the exploitation of the AV's inertia moments to perform maneuvers. By deliberately changing the rotational speeds around the three rotor axes, the AV can be rotated around its longitudinal, lateral, and vertical axes. This allows for rolling, pitching, and yawing of the AV.

A proposed method for utilizing gyroscopic forces during flight maneuvers is described here, which allows for the targeted control of the rotor's angular position about the pitch axis (y) and optionally also about the roll axis (x). To initiate changes in the orientation of the vehicle cell, moments must be generated through additional rotor unbalances. Two additional diametrical unbalance actuators, i.e., a pair per rotational axis (pitch, roll), are required for this purpose. For each of these axes, a positioning unbalance actuator is mounted on both the upper and lower deck surfaces of the rotor so that the radial directions of both unbalance actuators differ from each other by 180° (Figure 6 below). With anti-phase control, this adjustment results in inducing a dynamic unbalance of the rotor, causing a tilting of the main inertia axis to the rotor's axis of rotation. With exactly equal unbalance magnitudes on both the top and bottom rotor surfaces, the axes intersect at the rotor's center of gravity. The

centrifugal forces acting during rotation then generate a moment, which, for example, acts upon targeted control around the rotor's roll axis. If the vertical distance D between the two unbalance generators is equal to the thickness of the rotor disc and $2\alpha^*$ is the activation range of the dynamic unbalance, then an unbalance-induced moment $L = DR\ m_u{}^*\omega^2$ occurs for a short duration Δt during one rotation. The result is the precession of the rotor about the pitch axis (y axis), orthogonal to the roll axis (x). On the other hand, if a moment is generated around the pitch axis, the rotor has precession about the roll axis.

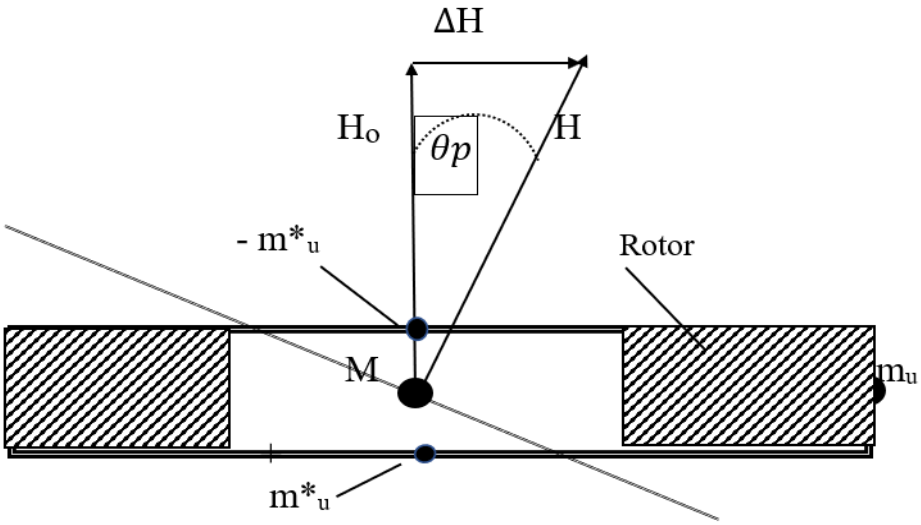

Figure 6. Rotor with actuators for the change in angular momentum. M, m_u, m_u*, mass points; θp, precession angle; H_0, H, angular momenta (before, after); ΔH, change in angular momentum.

For Method 2, the compensation for gyroscopic forces refers to mitigation of the undesirable effects of gyroscopic forces to ensure a stable flight attitude. This can be achieved through the use of sensors and control systems that adjust the rotational speeds of the rotors accordingly to compensate for unwanted rotations or vibrations.

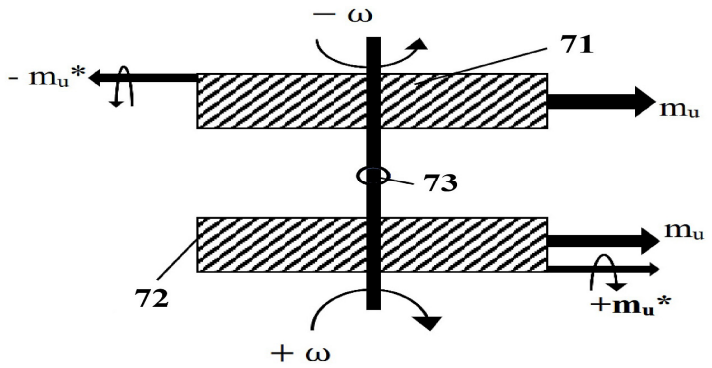

Figure 7. Counter-rotating rotor system. 71, Rotor; 72, counter-rotating rotor; 73, the system's center of mass; M, mu, mu*, mass points; ω, -ω, rotational angular velocities.

Compensation for gyroscopic forces in the entire system can be achieved by simultaneously operating two rotors arranged one above the other (Figure 7). Two identical rotors (91 and 92; twin rotors) rotate about the same axis of rotation (shaft) but in opposite directions. Each of the rotors is equipped with at least one unbalance actuator for propulsion. Such a twin rotor system provides double thrust in the forward propulsion mode (x direction) when both unbalance actuators are in phase, because the same unbalance-induced centrifugal force acts on each rotor regardless of the rotor's direction of rotation. The required temporal/angular synchronization of the two counter-rotating rotors is achieved when the two unbalance actuators meet exactly in the forward propulsion direction (the aircraft's longitudinal axis x) at the same time.

For initiating changes in the orientation of the vehicle cell, additional moments must be generated; for each axis of rotation (pitch, roll), an additional diametrical pair of unbalance actuators is required. A peripheral actuator is located on the upper rotor's top surface, with another peripheral actuator on the lower rotor's bottom surface but diametrically opposed to the upper one. A moment around the selected axis is created because, during each rotation of the rotor, the radial direction of these additional unbalance generators differs from each other by 180° at the right time. As a result of the anti-phase control, a dynamic unbalance of the rotor system is induced, causing a tilt of the main inertia axis to the common axis of rotation. With exactly equal unbalance magnitudes for both rotors, these axes intersect at the center of gravity (73) of the twin rotor system on the common axis of rotation, midway between the rotor discs (Figure 7).

To compensate for gyroscopic forces, a moment must be generated directly about the lateral axis for a pitching motion, and another moment must be generated directly about the longitudinal axis of the aircraft for a rolling motion. For yaw motion, in both cases, essentially only a "virtual" moment around the spin axis z is required. Specifically, within the rotor plane during a rotor's rotation, a controlled shift of the bisectors of propulsion in or against the rotor's rotational directions moves the system towards the desired new flight direction.

In our patent pending /25/, it is shown in more detail how the maneuverability around all three axes of the UAV can be optimized. The patent specification demonstrates how the two methods can be combined to optimize the maneuverability of the UAV. By strategically utilizing gyroscopic forces and compensating for the undesirable effects, precise and stable maneuvers can be performed.

Let us now assume a rotor-driven AV in vertical takeoff and landing (VTOL) mode, i.e., the rotational axis of the rotor is pointing horizontally in Earth´s gravitational field. To find the rotational speed at which the centrifugal force compensates for the weight, we set

$m_u R (2\pi f)^2 = M g_E$

This leads to the hovering rotational speed

$$f^* = \{(M g_E) / (4\pi^2 m_u R)\}^{1/2}. \quad (36)$$

To calculate the specific frequency f^*, we substitute the given values for the medium rotor into the formula

$M = 10$ kg, $M = 10^4 m_u$ (thus $m_u = 1g$), $g_E = 9.81$ m/s^2, $R = 0.5$ m.

Substituting these values, we get

$f^* = \text{sqrt}\ \{(10^4 m_u)\ 9.81\ \text{m/s}^2) / (m_u \cdot 0.5\ \text{m} \cdot 4\pi^2)\}$.

Calculating this, we obtain

$f^* \approx 70.5\ Hz.$

Therefore, the desired frequency f^* is approximately 70.5 Hz (or 4243 rpm).

We need to consider that even during the hovering of the rotor, its rotational energy is consumed because at least the center of mass M is displaced from the axis of rotation by the following amount:

$$r = R\, m_u / M = 0.5\ \text{m}\ (10^{-4}) = 0.05\ \text{mm}. \tag{37}$$

This displacement occurs exactly f^* times per second during the rotor's operation.

To calculate the power consumed during the hovering of the rotor, we use the following formula:

$$P = f^* \, dE_{rot} \tag{38}$$

With the energy loss $dE_{rot} = M\, g_E\, r$, we have

$$P = f^* \, M\, g_E\, r. \tag{39}$$

We substitute the given parameter values for the hovering medium rotor. With 1 W = 1 kgm^2/s^3, the formula gives the power consumption (in Watts):

$P = (70.5\ \text{Hz})\ (10\ \text{kg})\ (9.81\ \text{m/s}^2)\ (0.05\ 10^{-3}\ \text{m}) = 0.346\ \text{W}.$

To calculate the time that the rotor can hover, we need to calculate the rotational energy reserve. The rotational energy E of a rigid body is given by the formula

$$E = (1/2)\ \theta\, \omega^2, \tag{40}$$

where θ is the moment of inertia and ω is the angular velocity. The moment of inertia of a cylinder (which is typically what a rotor is) is calculated using the formula

$$\theta = (1/2)\, MR^2, \tag{41}$$

where M is the mass and R is the radius.

The angular velocity ω_0 is equal to $2\pi f_0$, where $f_0 = 400$ Hz is the assumed starting frequency. Substituting the given values into the formulas gives

$\theta = (1/2)\ 10\ \text{kg}\ (0.5\ \text{m})^2 = 1.25\ \text{kg m}^2$

$\omega_0 = 2\pi\ 400\ /s = 800\pi\ /s = 2{,}512\ /s$

Now we calculate the rotational energy

$E = (1/2)\ 1.25\ \text{kgm}^2\ (2512\ /\text{s})^2 = 3,\ 943,\ 840\ \text{J}.$

The time that the rotor can hover is thus the stored rotational energy divided by the power:

$$t = E / P = 3{,}943{,}840\ J / 0{,}346\ W = 11{,}398{,}381 s. \tag{42}$$

That is approximately 132 days.

This calculation is a strong simplification. In real rotor systems, additional factors such as friction, air resistance, and other losses can dominate and need to be taken into account as well.

6. Precise control in activating and deactivating rotor unbalances

The timing and magnitude of the unbalanced mass must be adjusted to optimize the generation of propulsion. To achieve precise control of the unbalanced mass, advanced control systems can be used. These systems monitor the rotational position of the rotor and activate electromechanical actuators to release or adjust the unbalanced mass at the desired time and magnitude [18]. Electrically controllable actuators [19] are fixed on the rotor, which apply the piezoceramic length expansion effect (PCT) or the magneto-strictive length expansion effect. The local direction of the length expansion effect must be aligned with the local radial direction of the rotor, causing controlled mass displacement effects towards the rotor's periphery and thus causing controlled unbalance (Figure 8).

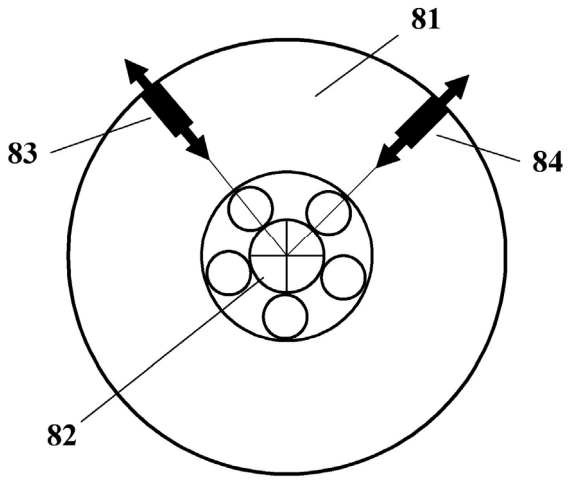

Figure 8. Actuator-based generation of rotor unbalance (example application). 81, rotor disc; 82, rotor bearing; 83 and 84, unbalance actuators for a fixed rotor.

The characteristic feature of applying PCT is that the energy requirement for the permanent modulation of the piezoelectric unbalance generator is low because the generator can work almost powerlessly due to the high internal resistance of PCT. Furthermore, the piezoelectric effect allows for rapid changes in unbalance. Possible PCT length changes are in the order of a few 100 µm, with mechanical response times of only 10^{-4} s or less. The characteristic feature of the piezoelectric unbalance generator is that rotations with frequencies of 10 kHz and higher become technically possible. Therefore, we conclude that by applying rotors equipped with current bearing technology, the unbalance control could be realized up to rotor speeds of about 1000 rps, and even higher speeds are possible for magnetically levitated rotors. Note that during accelerated flight, only unbalance-induced inertial forces act on the rotor bearing, as the elastic support forces are eliminated when the rotor's fixation is released. As a result, the load on the bearings due to unbalance is significantly smaller during flight compared with the operation of a tethered rotor. This is expected to have a favorable effect on the service life, especially for roller bearings.

Other possibilities that are usable for unbalance modulation are the piezoceramic longitudinal expansion effect (PCT actuators or PCT motors with a high actuating force and a high reaction speed)

or the magneto-strictive effect (large linear stroke) in solid bodies. In both cases, electrically controlling the position of the unbalanced mass is achieved along the length of the actuators. The actuators (83, 84) are located peripherally, fixed to the rotor, so that their action direction corresponds to the respective radial direction. The electric control voltage then locally causes activation or deactivation of the rotor's unbalance, depending on which actuator is driven at the time.

Figure 9 shows an image of the unbalance-generating actuator, which operates on the basis of the piezoelectric effect in piezoceramics (PCT). Two aligned PCT stack actuators (903, 904) and the unbalance-generating mass (902), made of, for example, tungsten alloy due to its high specific density, are clamped inside the rigid actuator housing (901) such that the center of gravity of the arrangement lies in the middle of the mass (902) on the axis of symmetry AA. As a result of this symmetric clamping, a mechanical stress field is generated in both the PCT actuators (903 and 904) and in the material block of the mass (902), acting perpendicular to the end faces of the three blocks. Due to this purely mechanical preloading, the direct piezoelectric effect causes the appearance of two DC voltages (V65 and V87) at terminal pairs 5 and 6, and 7 and 8, which are tapped from the respective end elements of the piezo stacks (903 and 904). When the same PCT material and the same geometric dimensions are used, these voltages are of equal magnitude due to the symmetry of 903 and 904, i.e., V65 = V87 = V0, where V0 defines the electrical operating point of the unbalance generator. The mechanical preloading additionally prevents undesired tensile loads from acting on the PCT stacks (903 and 904) during operation, which could potentially destroy them.

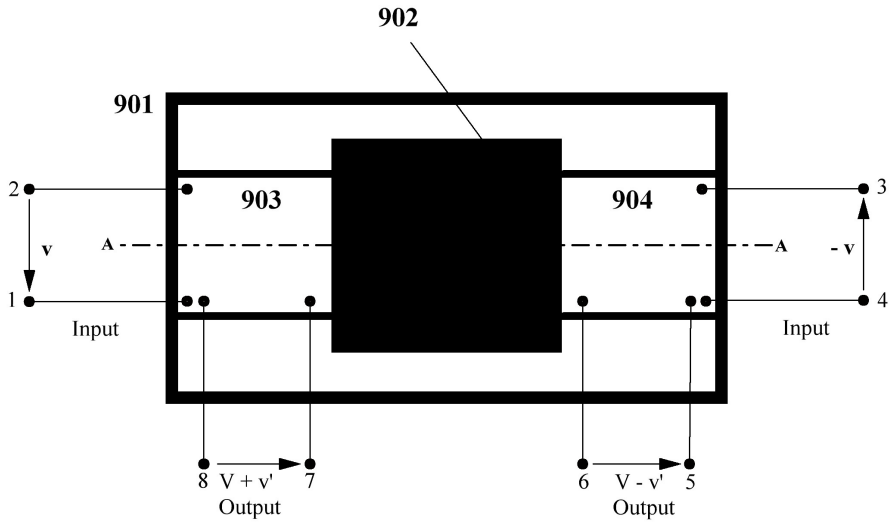

Figure 9. Unbalance actuator with steering voltages V, v.

One characteristic of the unbalance generator is that it simultaneously utilizes the direct piezoelectric effect and its inversion, the so-called inverse piezoelectric effect, in order to control the generation of unbalance. By applying an additional electric voltage (v21 or v43) to terminal pairs 1 and 2, and 3 and 4, the inverse piezoelectric effect causes an additional elongation or compression of the piezo stacks (903 and 904), also in the axis direction AA. The elongation or compression depends on the magnitude and sign of these controlling voltages (v12 and v34). This allows for a controlled displacement of the mass (902) along the axis AA and thus the generation of unbalanced mass. It is

also characteristic that the two PCT stacks (903 and 904) operate in an anti-phase manner, i.e., v12 = -v43 = v, meaning that one block elongates in the axis direction while the other block shortens by the same amount. This maintains the mechanical preloading and the operating point V0 while simultaneously creating space for a displacement of the mass (902) along the axis AA. This electrically induced displacement approximately results in an unbalanced mass of size $m_u = a^2 \partial l\, d$. Here, ∂l is the change in the length of the piezo stack or the displacement of the mass (902), a^2 is the cross-sectional area of the stack, and d is the dominant material density of the mass (902). If the radially oriented unbalance generator is located in a peripheral position at a distance R from the rotor's axis, the unbalance value $U = m_u R$ results as the mechanical output of the unbalance generator.

At terminal pairs 5 and 6, and 7 and 8, when the control voltages (v12 and v34) are applied in addition to the voltage V, an electrical voltage v' arises, which depends on the control voltage v. This voltage v' can be used for sensory size control of the generated unbalance U of the generator, which is characteristic of it. In small signal operation (i.e., as long as the unbalance-inducing electrical voltage v remains much smaller than the electrical bias voltage V0), the control voltage v' is directly proportional to the control voltage v and therefore is also proportional to the generated unbalance value U. Calibration of the measurable quantities unbalance value U or the displacement versus control voltage v or versus the control voltage v' yields the characteristics U = U(v) or U = U(v') for the necessary control in general. For the generation of propulsion through pulse modulation of the rotor unbalance, timing of the control voltage v realized with the rotation angle ω t is then required.

One characteristic is that the energy requirement for the permanent modulation of the piezoelectric unbalance generator is low, as this can be highly power-efficient due to the high inner resistance of PCT. By means of the piezoelectric effect, fast changes in unbalance can be induced with the dielectric unbalance generator. Possible changes in the PCT's length are in the order of several 100 μm, with mechanical reaction times of only 10^{-4}s or less. Another characteristic of the piezoelectric unbalance generator is that modulation with frequencies of 10 kHz and higher becomes technically feasible. Therefore, we conclude that with the current rolling bearing technology, unbalance control can be implemented up to rotor speeds of about 1000 revolutions per second; even higher speeds are possible for magnetically supported rotors.

Further variations of unbalance generators are feasible, such as those with PCT bending elements instead of PCT stacks, with magneto-strictive actuators or with other materials instead of the heavy metal tungsten. An arrangement without the central mass (902) in a simple but highly dynamic design is also conceivable, in which the mass displacement is solely achieved through a shift in the center of gravity of the PCT actuator.

7. High-strength rotor materials

For high-speed rotors, materials with high tensile strength and low material density are essential. In designing a propulsion system, the following criterion of strength theory must be considered: In a high-speed rotating rotor (balanced), the tangential component of the surface stress s_t must not exceed the tensile strength of the rotor material

$$s_t = \rho\, v^2_R < \text{maximum tensile strength } s_{max}. \tag{43}$$

The component of the surface stress s_t itself is proportional to the material density ρ and the square of the circumferential velocity v_R of the rotor. This is determined by

$$v_R = 2\pi R f. \tag{44}$$

Therefore, we have

$4\,\rho\,\pi^2 f^2 R^2 < s_{max}$

$$f\,R < (1/2\pi)\,(s_{max}/\rho)^{(1/2)}. \tag{45}$$

This formula says that the optimized rotor material should have a tensile strength s_{max} as large as possible and its density ρ should be as low as possible. Rotors built by using this optimized material allow large magnitudes of the critical product f R, i.e., high rotation frequencies f in combination with the large radius R of big rotors. The permissible tensile strength should include additional stresses induced by the centrifugal force of the unbalanced mass.

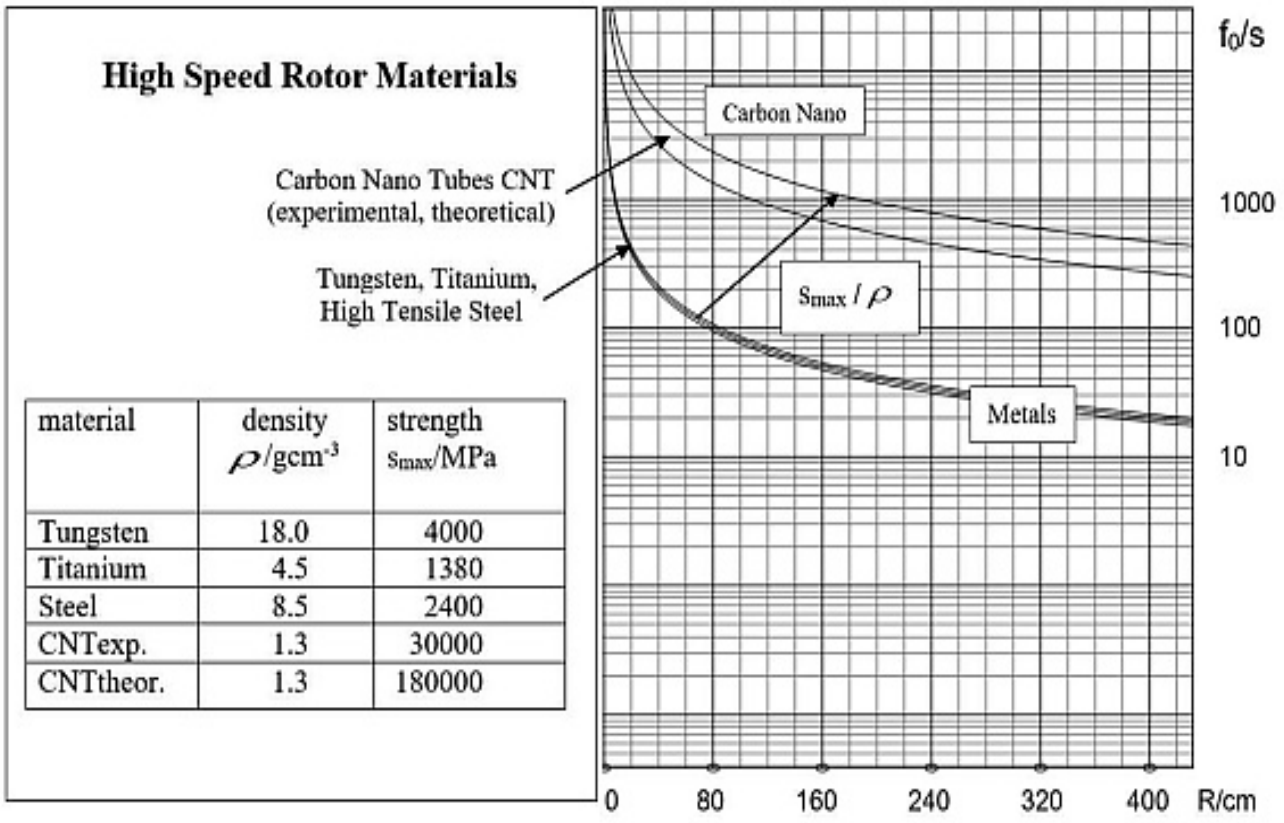

material	density ρ/gcm^{-3}	strength s_{max}/MPa
Tungsten	18.0	4000
Titanium	4.5	1380
Steel	8.5	2400
CNTexp.	1.3	30000
CNTtheor.	1.3	180000

Figure 10. The highest rotational frequencies f_0/s dependent on the radius R and the parameter s_{max}/ρ for selected materials according to Eq 45. Material data have been taken from [20–23].

Our calculation results for some metallic materials and for carbon nanomaterials are shown in Figure 10. We draw the following conclusion: Using the present metallic rotor materials, radii in the

submeter range can be achieved for speeds of 100–1000 rps, especially with carbon-fiber-reinforced polymer (CFRP)-wrapped steel rotors, like those described in [20]. Furthermore, on the basis of some success in earlier experiments with nanomaterials [20–22], single-walled carbon nanotubes theoretically possess ultimate intrinsic tensile strengths in the 100–200 GPa range, which are among the highest in existing materials. We are therefore free to state that the highest rotor speeds (1000 rps) could be achieved when using ultra-stable carbon nanomaterial structures because this technology could be combined with allowable rotor radii in the order of several meters. Let us compare these demands with the state-of-the-art rotor equipment: CNC tool machine spindles (80 mm) allow 250 rps, standard commercial high-speed ball bearings perform at 350 rps, and magnetic bearings work up to 500,000 rpm and more; see [14,24].

8. Some aerodynamic aspects of rotor-driven aerial vehicles

In order to enable vertical takeoff like a rocket and ensure that forward thrust acts upwards (vertically) even without aerodynamic aids, the axis of rotation must lie in the horizontal plane and the gravitational acceleration g_E must be constantly overcompensated (see Section 5). This VTOL mode requires a sufficiently large vertical (upward) centrifugal force component of the rotor disc. A horizontal axis position also allows for a safe landing without additional aerodynamic aids.

Here, it may be of interest to discuss the aerodynamic lift of rotor-driven aerial vehicles. Starting and landing procedures as well as midflight maneuvering can also be performed through the simultaneous combination of rotor thrust and aerodynamic aids. Speed-dependent lift is generated if the thrust force of the unbalanced rotor acts horizontally.

(a) The aerodynamic shape of the aerial vehicle corresponds to the common aircraft form, but without external engines. The rotor drives are located in the wings or fuselage. If, as in Figure 11, gyroscopic moments are compensated for, maneuverability in flight can be achieved through the usual aerodynamic control surfaces. Higher thrusts by means of pulse-modulated force propulsion can be created because instead of using a single super rotor with a large radius, a battery of several smaller rotors (mounted on a common vehicle platform) can be applied and operated with synchronous unbalance control so that the individual propulsion forces add up.

(b) A circular symmetrical cell (121, nonrotating) with suitable aerodynamic shaping contains the rotor drive (122) (see Figure 11). This special circular disc (121) has the so-called isotropic aerodynamic profile, which means that all (virtual) vertical cuts containing the rotor axis (125) of the cell (121) result in an identical shape, for instance, that of Figure 8. Such highly isotropic disc-shaped cells should allow total maneuverability (horizontal thrust direction variable within 0–360°) due to their rotationally symmetrical design.

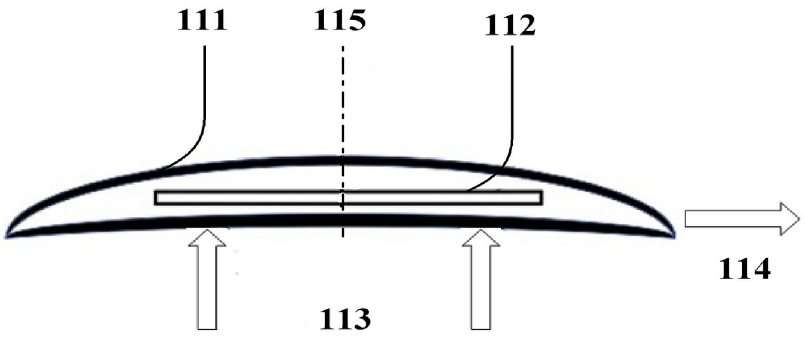

Figure 11. Aircraft cell (111) with an aerodynamic profile and an internal rotor disc (112) with a controlled unbalanced mass. Aerodynamic lift force, 113; translational propulsion of the vehicle cell, 114; the rotor's axis of rotation, 115.

Therefore, in both cases (a, b), a certain takeoff distance is required for successful horizontal starts. Furthermore, it must be determined principally whether the required aerodynamic stability can be better achieved through gyroscopic effects or additional aerodynamic surfaces.

9. Discussion and final conclusion

In this paper, we have introduced a deeper insight into using controlled unbalance propulsion (CUP) for electrical thrust generation in aerial vehicles. This proposed technique is firmly grounded in established principles of physics and can be implemented using current advanced technologies. Through CUP, the rotational energy of a rotor can be effectively converted into the translational energy required to propel the vehicle. Our mathematical model of CUP aircraft with rotor propulsion demonstrates the following:

- It shows the dependence of thrust on key system parameters;
- It enables predictions of Avs' flight performance;
- It provides guidance for the structural design of aircraft;
- It allows for targeted validation through experiments;
-It should offer a decision for or against the classical interpretation of fictitious forces.

Our numerical calculations based on this theory suggest the potential for achieving very high flight performance, especially in the case of small UAVs. Our systematic study recognizes the advantageous characteristics of the rotor drive: This drive should enable high translational acceleration and velocities, extreme maneuverability, VTOL, and hover capability. It operates with purely electric/inertial energy storage and is completely emission-free, meaning there is no emission of combustion gases, liquids, particles, etc. Furthermore, the rotor drive can be utilized in principle in the atmosphere, in space, on the Earth's surface, on water, and also underwater. By applying a capsuled vehicle, transmedia transitions (i.e., underwater–atmosphere and vice versa) also seem possible.

What about the pseudo-force nature of centrifugal forces? In many areas of modern physics, the so-called Noether theorem significantly large importance, not only in classical mechanics. It states that for every continuous symmetry in a physical system, a conservation quantity follows. For example, the conservation of angular momentum for a rotor follows from the isotropy of space. On the other hand, if the symmetry is broken, the corresponding conservation law no longer applies.

The use of CUP to generate propulsion requires – as outlined above – the temporary generation of periodic unbalances during each rotor revolution. However, each unbalance also destroys the (azimuthal) mass symmetry in the rotor system, meaning that, due to the Noether theorem of physics, the law of angular momentum conservation no longer holds for an unbalanced rotor system. Therefore, there is also no "pseudo-force" problem anymore, as the symmetry is broken and the force caused by the unbalance can work to accelerate the rotor's mass. Consequently, the rotational energy is continuously reduced, which means that the rotational frequency decreases. As a result, the angular momentum of the rotor must also continuously decrease because the conservation law no longer applies. Thus, the CUP theory is not in contradiction to physics but rather follows from it.

Overall, we present tangible evidence that it is essential now to initiate experiments and conduct in-depth system analyses to validate the feasibility and efficiency of the proposed propulsion method. Furthermore, systematic studies on AVs with integrated electrical onboard rotor drives have to be performed for further clearing up the performance potential of rotor drives.

Hereby, we believe in the phrase "We must know and we shall know!" (mathematician David Hilbert, Paris 1900).

Use of AI tools declaration

The author declares that he has used Artificial Intelligence for language checking. AI was not involved in the creation of scientific results presented in this paper.

Acknowledgments

The author thanks Dipl.-Ing. Helmut Lotz (VDI Kassel) for his helpful assistance in illustrating this paper.

Conflict of Interest

The author declares no conflicts of interest.

References

1. Holzapfel W （2024) Pulsed Propulsion of Unmanned Aerial Vehicles by Centrifugal Force Modulation—First-Order Theory and Practicability. *Appl Sci* 14: 4229. https://doi.org/10.3390/app14104229
2. Skowronski MJ (2018) Impulse Momentum Propulsion Apparatus and Method. US Patent 2018 000551 A1.

3. Henry William Wallace (1987) Gyroscopic Propulsion. US-Patent 4,663,932
4. Sandy Kidd (1980) Gyroscopic Propulsion Device. US-Patent 4,238,968
5. Bowen Zhang, Zaixin Song, Fai Zhao, et al. (2022) Overview of Propulsion Systems for Unmanned Aerial Vehicles. *Energies* 15*:* 455. https://doi.org/10.3390/en15020455
6. Dhawal Joshi, Dipankar Deb, SM Muyeen, et al. (2022) Comprehensive Review on Electric Propulsion System of Unmanned Aerial Vehicles. *Front Energy Res* 10: 752012. https://doi.org/10.3389/fenrg.2022.752012
7. Drone - Unmanned Aerial Vehicle (UAV) 2020–2023 Safe Drones over Save Environment Tempus Foundation Erasmus + 2020-1-RS01-KA202-065370 HANDBOOK
8. Faraji F, Majazi A, Al-Haddad K (2017) A comprehensive review of Flywheel Energy Storage System technology. *Renew Sust Energ Rev* 67: 477–490. https://doi.org/10.1016/j.rser.2016.09.060
9. Li X, Palazzolo A (2022) A review of flywheel energy storage systems: state of the art and opportunities. *J Energy Storage* 46: 103576. https://doi.org/10.1016/j.est.2021.103576
10. YU S, GUO W, TENG Y, et al. (2021) A review of the structures and control strategies for flywheel bearings. *Energy Storage Sci Technol* 10: 1631–1642. https://doi.org/10.19799/j.cnki.2095-4239.2021.0237
11. Karrari S, De Carne G, Noe M (2021) Model validation of a high-speed flywheel energy storage system using power hardware-in-the-loop testing. *J Energy Storage* 43: 103177. https://doi.org/10.1016/j.est.2021.103177
12. Karrari S, Noe M, Geisbuesch J (2018) Real-time simulation of high-speed flywheel energy storage system (FESS) for distribution networks. In: *Proceedings of the Ninth International Conference on Future Energy Systems*, 388–390. https://doi.org/10.1145/3208903.3212034
13. Flywheel Generators (2021) Max Planck Institute for Plasma Physics. https://www.ipp.mpg.de/generator
14. Buchroithner A (2023) Automotive Engineering, In: *Flywheel Energy Storage*. Springer. https://doi.org/10.1007/978-3-658-35342-1
15. Halliday D, Resnick R, Walker J (2013) *Fundamentals of Physics*. Hoboken, NJ: John Wiley & Sons, 1456. ISBN 9781-1-118-34140
16. Taylor JR (2005) Classical Mechanics. Sausalito, CA: University Science Books. 1st edition. ISBN-10: 189138922X, ISBN-13: 978-1891389221. 802.
17. Demtröder W (2010) Physik für Ingenieure 4. Auflage 2010, Springer-Verlag, 630. ISBN 978-3-642-15092-0
18. Schneider H (1992) *Auswuchttechnik*. Springer Verlag. ISBN 978-3-540-56117-7.
19. Zhog Lin Wang, Yan Zhang Weiguo Hu (2023) Applications to Third Generation Semiconductor Microtechnology (Microtechnology and MEMS). Springer, ASIN: B0C3WZNKY8.
20. Bai Y, Zhang R, Ye X, et al. (2018) Carbon nanotube bundles with tensile strength over 80 GPa. *Nat Nanotech* 13: 589–595. https://doi.org/10.1038/s41565-018-0141-z
21. Takakura A, Beppu K, Nishihara T, et al. (2019) Strength of carbon nanotubes depends on their chemical structures. *Nat Commun* 10: 3040. https://doi.org/10.1038/s41467-019-10959-7
22. Ruoff RS (2018) Strong bundles based on carbon nanotubes. *Nat Nanotech* 13: 533–534 https://doi.org/10.1038/s41565-018-0184-1

23. Cambridge Engineering Selector software (CES 4.1), 2003, Granta Design Limited, Rustat House, 62 Clifton Rd, Cambridge, CB1 7EG (Materials Data).
24. Schuck M, Steinert D, Nussbaumer T, et al. (2018) Ultrafast rotation of magnetically levitated macroscopic steel spheres. *Sci Adv* 4: e1701519. https://doi.org/10.1126/sciadv.1701519
25. Wolfgang Holzapfel (2023) Verfahren zur Vortriebserzeugung. Patent pending. Deutsches Patent und Markenamt. Available from: https://patentimages.storage.googleapis.com/eb/a8/d5/9ecab7c4cc0447/DE102021004170A1.pdf.

AIMS Press